Athens Institute for Education and Research
ATINER

ATINER's Conference Paper Series
CIV2014-0971

Non-linear FE Modelling of CFRP-Strengthened RC Slabs under Cyclic Loading

Raid Daud
PhD Candidate, University of Manchester, UK
Lecturer, Alnahrain University, Iraq

Lee Cunningham
Lecturer
University of Manchester
UK

Yong Wang
Professor
University of Manchester
UK

An Introduction to ATINER's Conference Paper Series

ATINER started to publish this conference papers series in 2012. It includes only the papers submitted for publication after they were presented at one of the conferences organized by our Institute every year. The papers published in the series have not been refereed and are published as they were submitted by the author. The series serves two purposes. First, we want to disseminate the information as fast as possible. Second, by doing so, the authors can receive comments useful to revise their papers before they are considered for publication in one of ATINER's books, following our standard procedures of a blind review.

Dr. Gregory T. Papanikos
President
Athens Institute for Education and Research

This paper should be cited as follows:
Daud, R., Cunningham, L. and Wang, Y., (2014) **"Non-linear FE Modelling of CFRP-Strengthened RC Slabs under Cyclic Loading"**
Athens: ATINER'S Conference Paper Series, No: **CIV2014-0971.**

Athens Institute for Education and Research
8 Valaoritou Street, Kolonaki, 10671 Athens, Greece
Tel: + 30 210 3634210 Fax: + 30 210 3634209
Email: info@atiner.gr URL: www.atiner.gr
URL Conference Papers Series: www.atiner.gr/papers.htm
Printed in Athens, Greece by the Athens Institute for Education and Research.

ISSN: **2241-2891**
23/6/2014

Non-linear FE Modelling of CFRP-Strengthened RC Slabs under Cyclic Loading

Raid Daud
PhD Candidate, University of Manchester, UK
Lecturer, Alnahrain University, Iraq

Lee Cunningham
Lecturer
University of Manchester
UK

Yong Wang
Professor
University of Manchester
UK

Abstract

The nonlinear behaviour of an adhesive layer connecting carbon fibre reinforced polymer (CFRP) to reinforced concrete one way slabs is numerically simulated in the current study. This investigation is aimed at developing as well as validating a three-dimensional finite element model. Numerical results have been compared with those obtained from an earlier experimental study. The FE model was then subjected to the modified fatigue load protocol recommended by FEMA 461. A detailed and accurate 3D FE model of the composite one-way slab was developed using ABAQUS software. A non-linear damage plasticity model is considered for modelling the concrete, and the FE model accounted for the nonlinearity of the concrete under cyclic loading by estimating the stiffness degradation in the concrete for both compression and tension effects. A surface cohesive based model was used to describe the interaction between the CFRP and the concrete slab. For the reinforcement bars, the Bauschinger effect was adopted through the application of the kinematic hardening model under cyclic loading. The FE model was then validated by comparing numerical and experimental values for load-deflection, load-strain in CFRP and load-strain in embedded reinforcement bars. Furthermore, the strain profile of CFRP, slip at interface in monotonic and cyclic loading, and both reduction in the ultimate load and stiffness due to cyclic loading were observed in this study.

Keywords: Adhesive layer, CFRP, Fatigue, Finite elements, Reinforced concrete.

Acknowledgments: Our thanks to "*The Higher Committee for Education Development in Iraq*" for funding this research. Sincere thanks are expressed to *School of Mechanical, Aerospace and Civil Engineering* of the University of Manchester for providing the facilities to undertake this research.

Introduction

The reliability of the bond is crucial to the performance of reinforced concrete (RC) members externally strengthened with fibre reinforced polymers (FRP) under monotonic and cyclic loading. The force transfer mechanism at the interface between the FRP composite sheet and concrete is dependent on the quality of the adhesive layer. The adhesive layer connecting the FRP-concrete composite consists of an effective mechanism for resisting the shear force at the interface between FRP and the concrete slab. Hence, enhancing the bond promotes the extension of service fatigue life of FRP-strengthened RC elements, as well as increasing their load bearing capacity. A good knowledge of the nonlinear behaviour of the adhesive interface is vital for controlling the design of FRP-strengthened RC slabs.

Many studies have experimentally investigated the nonlinear behaviour of RC members, strengthened with FRP under monotonic loading [1-2] or through numerical modelling [3-4]. Other studies have also investigated the behaviour of RC members strengthened by FRP under cyclic loading [5-6]. Analytical models are also available to account for the interfacial behaviour between the FRP laminates and the concrete slab [7].These Analytical models are useful for obtaining a good prediction of the load displacement behaviour observed experimentally.

It is well-known that several finite element models [8-9] have been developed for investigating carbon fibre reinforced polymer (CFRP)-strengthened RC slabs subjected to monotonic loading by imposing the interface behaviour. However, the need to understand the actual interface behaviour in CFRP-strengthened RC slabs under cyclic loading still exists. The study of the nonlinear behaviour of RC members strengthened with CFRP, using the finite element method (FEM) often entails some fundamental assumptions [10]. One of such assumptions is the insertion of both the tension and compression damage parameter for estimating the stiffness degradation in the concrete for both compression and tension, due to cyclic effects. Another important assumption is to impose the Bauschinger effect for steel reinforcement bars, through the application of the kinematic hardening model. Also, the traction-separation based model is another assumption that defines the material properties of the adhesive layer with a degraded cohesive stiffness, when the stresses at the contact point satisfy maximum nominal stress criterion. By applying these assumptions, the predictions from the 3D-FEM can closely match those from experimental observations.

Elsayed W. et al [7] modelled two way concrete slabs using 3D brick elements; truss elements to model reinforcement bars; and 2D shell elements to represent the FRP laminates. The FRP/concrete interface was then modelled using a spring element. This model was unable to capture the actual nonlinear interface behaviour under cyclic loading for the following reasons: (1) The spring element is unable to trace the unloading and reloading paths, (2) The damage evolution behaviour is always inserted as load slip therefore, it cannot

estimate the interface stiffness degradation induced fracture energy release due to cyclic loading.

In the current study, emphasis is placed on understanding the nonlinear behaviour of an adhesive layer connecting CFRP to RC one-way spanning slabs, through detailed finite element (FE) simulation. Using the commercially available software ABAQUS, a 3D FE model of CFRP-strengthened RC slabs under cyclic loading was developed, and then validated using the results from earlier experimental work by Arduini et al. [11]. In the experiment [11], a series of nine full-scale one-way RC slabs (with and without externally bonded unidirectional CFRP) under simply supported conditions were subjected to two cycles. For the first cycle, the load reached 1/3 of the nominal capacity. In the second cycle, the specimen was taken to failure. Specimen characteristics and the test configuration are shown in Figure.1. Herein this paper describes the FE model, material properties, interface behaviour, and a comparison of the earlier experiment with the current analysis. Additional analysis was conducted by modifying an existing standard cyclic loading protocol, so as to obtain the load deflection behaviour, slip and strain profiles.

Figure 1: *Details of CFRP-strengthened RC slab specimen. [11]*

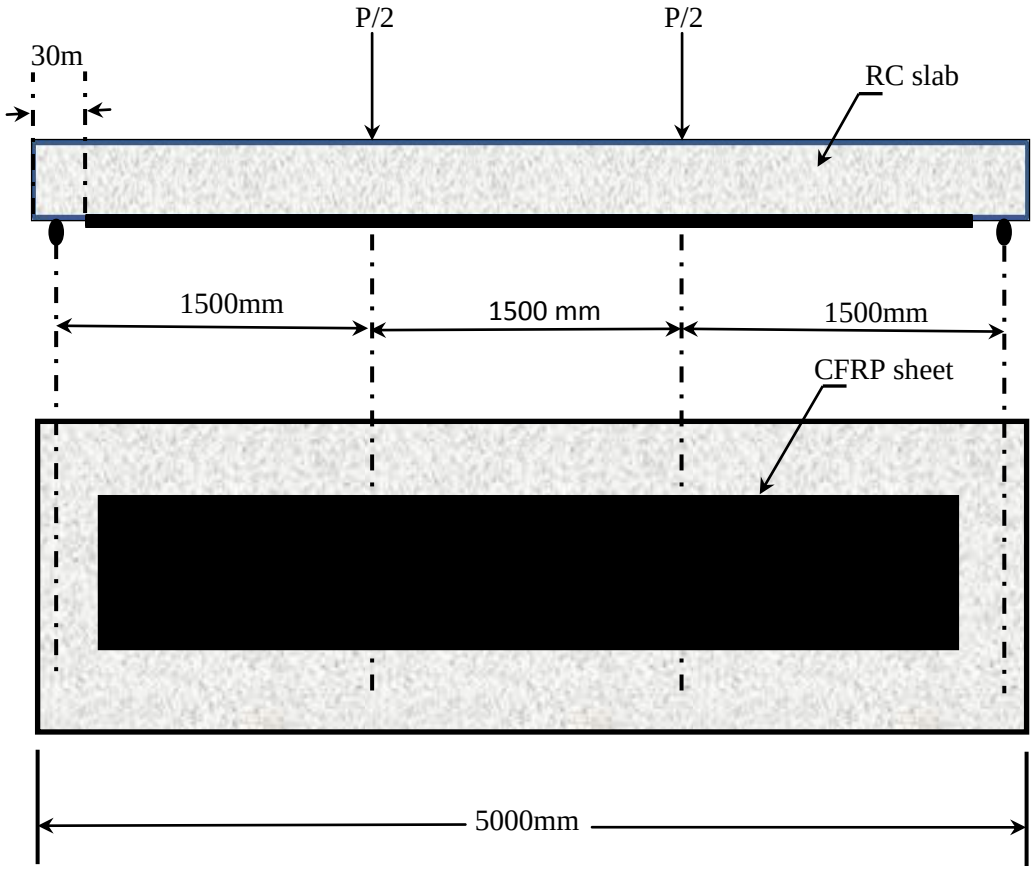

Finite Element Model

Figure 2 shows the FE model of the simply supported CFRP-strengthened RC one-way slab with a clear span of 4.5 m as modelled using the ABAQUS software. The test load was applied as a uniform pressure on the top surface of the steel bearing plate (2.5 mm width and 1500 mm length, which is equivalent to the full width of the slab, so as to uniformly distribute the load across the concrete surface). In order to minimise computational burden, only a quarter of the slab has been modelled in the 3DFE analysis, although, all conditions (loading, boundary conditions and geometry symmetry) were properly accounted for, as shown in Figure.2.

Figure 2: *Quarter model of the CFRP-strengthened RC slabs*

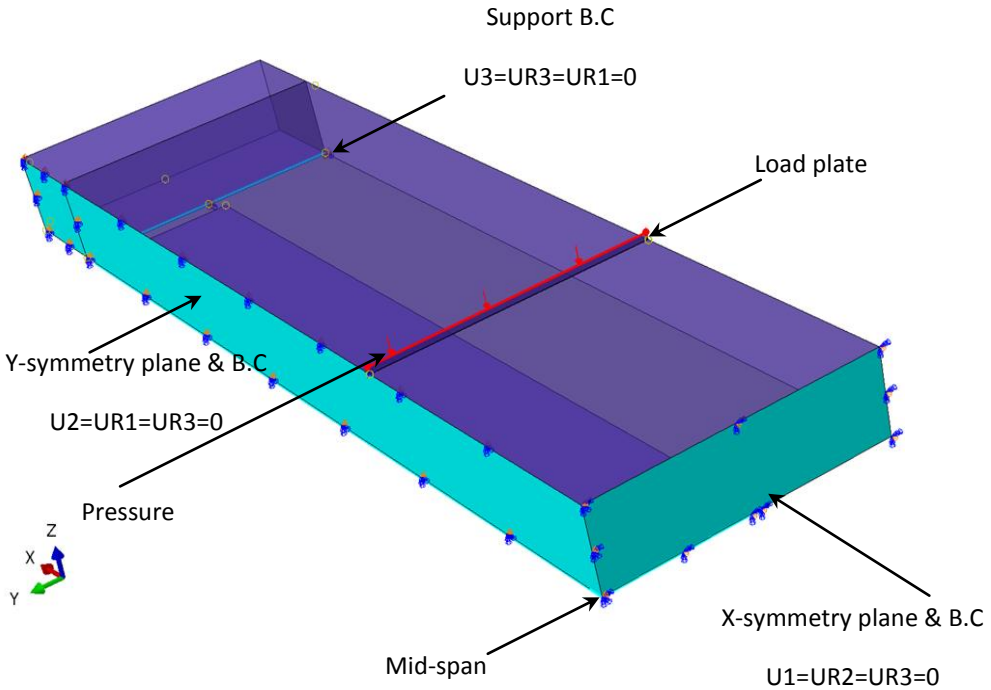

U: 1, 2, 3 = Translation in X, Y and Z directions respectively
UR: 1, 2, 3 =Rotation about X, Y and Z directions respectively

The restrained degrees of freedom at the symmetrical edge boundary conditions are also shown in Figure 2, where axes 1, 2, 3 represent the three coordinate axes xyz respectively. A convergence investigation was undertaken in order to decide what element type and mesh size is required at each instance, namely; concrete, reinforcement bars, CFRP as shown in Figure 3. Based on the convergence study, it was deduced that a 3D eight-node linear brick element with reduced integration and hourglass control (C3D8R) for modelling the concrete was most appropriate. For the embedded reinforcement bars, a linear 3D two node truss element with three degrees of freedom at each node

(T3D2) was used. The CFRP composite plate was modelled using linear 3D three-node triangular facet thin shell element (STRI3). The cohesive contact was applied between the CFRP and concrete slab using the cohesive surface technique, which is represented as part of the surface interaction properties that were assigned to a contact pair (adhesive thickness was negligibly small). A nonlinear static, general step was performed to analyse the current model. The basic algorithm of this analysis is the Full Newton method, where the numerical solution is defined as a series of increments with iterations to achieve equilibrium within each increment. Material and geometrical details of the RC slab strengthened with CFRP are provided in Tables 1 and 2 respectively.

Figure 3: *Finite element mesh of the quarter the CFRP-strengthened RC slabs*

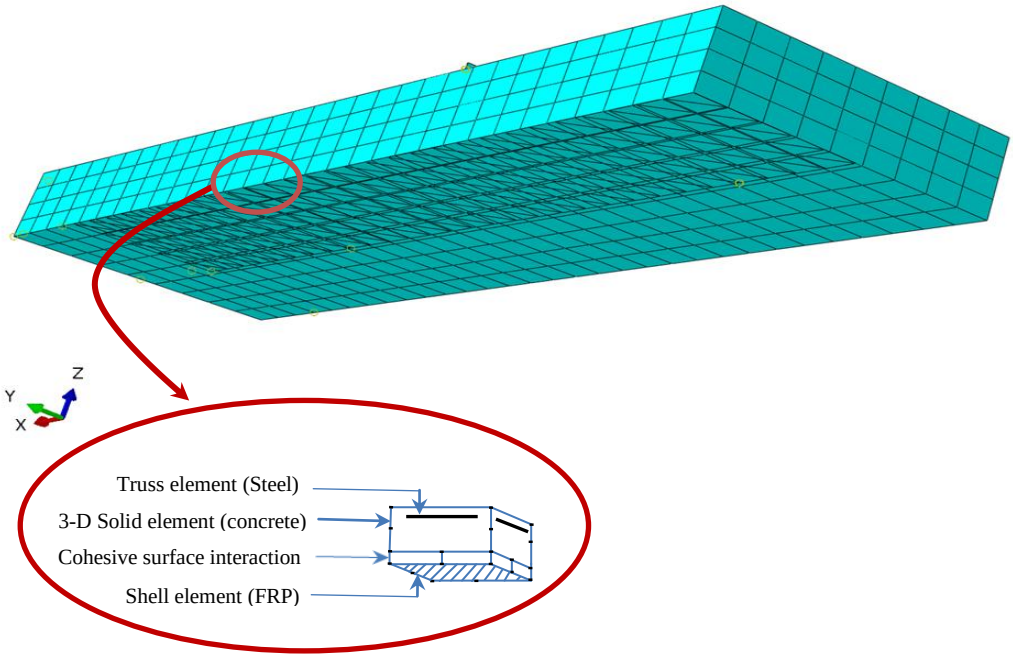

Table 1: *Details of materials used for slabs (S-T1)*

Material	Description	Value
Concrete	Elastic modulus, GPa	33
	Poisson's ratio	0.15
	Characteristic compressive strength(f_c), MPa	33
	Characteristic tensile strength(f_t), MPa	2.2
Reinforcement bars	Elastic modulus, GPa	200
	Poisson's ratio	0.3
	Yield strength of reinforcing bar (f_y), MPa	512
CFRP	Longitudinal modulus (E_1), Gpa	230
	*Transverse in-plane modulus(E_2), GPa	23
	*Transverse out-plane modulus(E_3), GPa	23
	*In- plane shear modulus (G_{12}), GPa	6.894
	*out- of-plane shear modulus (G_{23}), GPa	4.136
	*out- of-plane shear modulus(G_{13}),GPa	6.894
	*Major in -plane Passion's ratio, ν_{12}	0.3
	*Out-of-plane Passion's ratio, ν_{23}	0.25
	*Out-of-plane Passion's ratio, ν_{13}	0.25
	Characteristic tensile strength(f_t), MPa	3400

*: material properties are taken according to the reference Reddy, J. N [12]

Table 2: *Details of Geometry used for Slabs Type (S-T1)*

code	Dimension(m)	Tension steel		Compression steel		CFRP				Span L(m)
		N_s^* ϕ (mm)	ρ_s	$N_s'^*$ ϕ (mm)	ρ'_s	w_f (mm)	N_f	A_f (mm^2)	L_f (m)	
S-T1L0	5.0 x 1.5 x 0.24	8 ϕ 12	0.0027	8 ϕ 12	0.0027	0	0	0	0	4.5
S-T1L1						800	1	132	4.4	
S-T1L2						1500	1	247		

N_s^* ϕ(mm): number and reinforcing bar diameter, that is 8 ϕ 12 means 8 reinforcing bars 12 mm in diameter.

Loads

The line loading (Figure 2) has been applied as an equivalent pressure on the top surface of load plate over a concrete contact width of 2.5mm. The cyclic load was modelled using a modified load protocol recommended by FEMA 461[13]. The load protocol has been amended to use only the positive loading scenario, i.e. load reversal does not occur (Figure 4). This is more

characteristic of imposed floor loads on buildings or traffic loads on bridges (i.e. on/off loading as opposed to load reversal which is more associated with wind and seismic actions). This protocol is appropriate to low cycle fatigue where the maximum load amplitude of the cycle is greater than 50% of the member's ultimate load and where typically less than one million cycles are needed to induce failure of the member. In this load protocol, the first stage of the low fatigue cycle applies ten cycles of deformation amplitude i.e. Δ_1 = 0.1 of the ultimate deformation in the monotonic case, this is followed by three further cycles of amplitude 1.2 times the deformation amplitude in the first stage i. e. $\Delta_2 = 1.2\ \Delta_1$. In each of the subsequent stages, the deformation amplitude is increased by 0.2 (i.e. $\Delta_3 = 1.2\ \Delta_2$, $\Delta_4 = 1.2\ \Delta_3$,.., etc.), while subjecting the specimen to three cycles until complete damage.

Figure 4: *Load protocol: (a) FEMA461 (b) modified FEMA461*

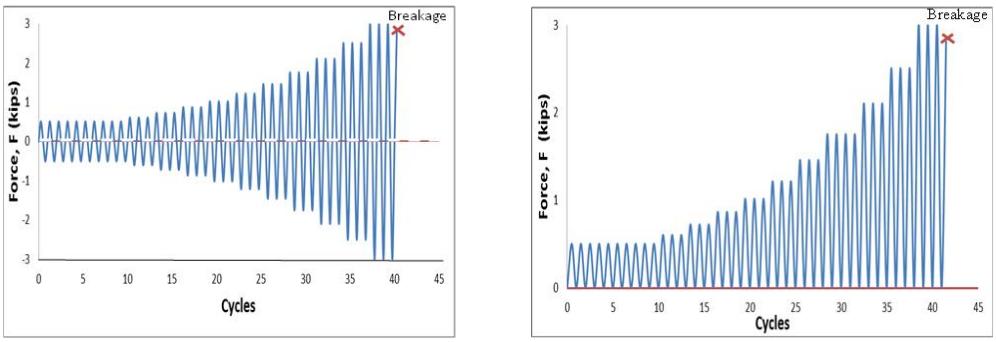

(a) (b)

Material Model

Concrete

Compression Behaviour

The uniaxial compressive stress-strain relationship for plain concrete after the elastic regime is defined. According to ABAQUS, setting both hardening and strain-softening range are defined in terms of compressive stress, σ_c and inelastic strain, $\tilde{\varepsilon}_c^{in}$ which is given as follows:

$$\tilde{\varepsilon}_c^{in} = \varepsilon_c - \varepsilon_{0c}^{el} \qquad (1)$$

where $\varepsilon_{0c}^{el} = \sigma_c / E_{cm}$, and E_{cm} is the initial modulus of elasticity

The FE analyses were conducted based on the uniaxial compressive concrete model of BS EN 1992-1-1:2004 Euro code 2 Design of concrete structures [14] as shown in Figure 5, is described by the expression

$$\frac{\sigma_c}{f_{cm}} = \frac{kn - n^2}{1 + (k-2)n} \quad (2)$$

$$n = \varepsilon_c \Big/ \varepsilon_{c1} \quad (3)$$

$$k = 1.05\ E_{cm} \times |\varepsilon_{c1}| / f_{cm} \quad (4)$$

It should be noted that the expression in equation (2) is valid for $0 < |\varepsilon_{c1}| < |\varepsilon_{cu1}|$ where ε_{cu1} is the nominal ultimate strain (0.0035); ε_{c1} is the strain at peak stress (0.0021); and f_{cm} is mean compressive strength.

Figure 5: *Uniaxial compressive stress-strain behaviour of concrete.*

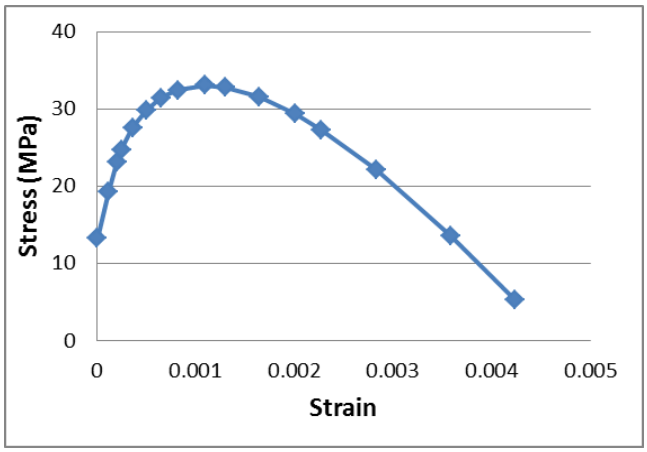

Tension Behaviour

The tension stiffening effect is considered owing to the fact that the cracked concrete will initially carry some tensile stresses in the direction normal to the crack. This can be performed by assuming a gradual release of the concrete stress component normal to the cracked plane. Exponential curves have been proposed to model tension stiffening. The current tension stiffening model shown in Figure 6 was obtained from Wang and Hsu [15].

$$\sigma_t = f_t \left(\frac{\epsilon_{cr}}{\epsilon_t}\right)^{0.4} \qquad \epsilon_t > \epsilon_{cr} \quad (5)$$

Figure 6: *Uniaxial tensile stress-strain behaviour of concrete*

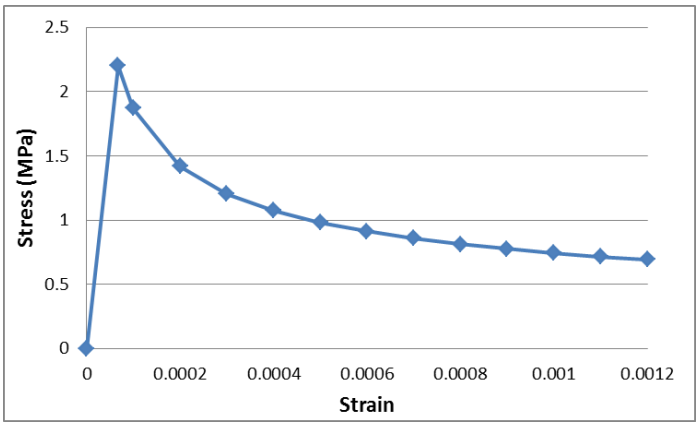

Principle of Concrete Damaged Plasticity Formulation

The most significant aspects of the damage plasticity model can be defined as compression and tension degradation. When the element plasticizes, the elastic stiffness becomes lowered by damage properties, thus it is unable to recover its initial elastic stiffness. This is substantial for cyclic loading, as the two damage parameters, d_c *and* d_t, which are assumed to be functions of the plastic strains, temperature, and field variables represent degradation of the elastic stiffness.

$$d_t = d_t\left(\epsilon_t^{\sim pl}, \theta, f_i\right); 0 \leq d_t \leq 1 \quad (6)$$

$$d_c = d_c\left(\epsilon_c^{\sim pl}, \theta, f_i\right); 0 \leq d_c \leq 1 \quad (7)$$

where the subscripts *t* and *c* refer to tension and compression respectively; $\epsilon_c^{\sim pl}$ and $\epsilon_t^{\sim pl}$ are the equivalent plastic strains; θ is the temperature; and $f_i, (i = 1, 2, \ldots..)$ are other predefined field variables [10]. The damage parameters can take values ranging from zero (characterizing the undamaged material), to one (characterizes total loss of strength). The default of damage plasticity can be illustrated using Figure 7

Figure 7: *Uniaxial load cycle (tension-compression-tension). [10]*

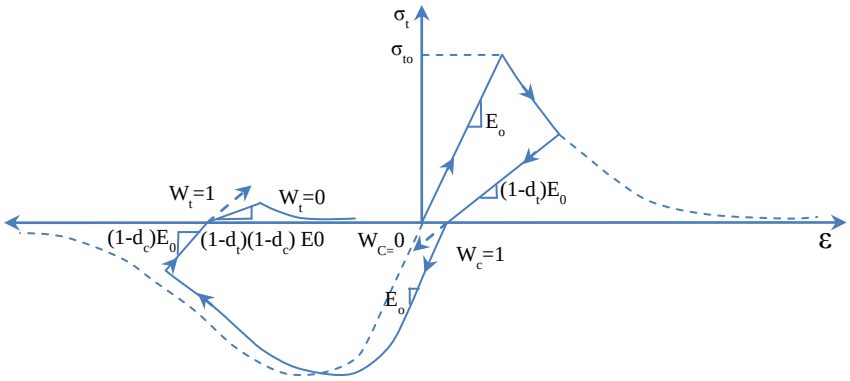

Figure 7 shows the basic tension and compression stress –strain curve as a dotted a line, while the solid line represents a high damage cyclic loading curve Tyau, J. S. (2009) [16] when the element is subjected to tension exceeding its tensile strength. Cracking however leads to partial damage of the material, and can be denoted by the variable d_t. The elastic behaviour of the element after unloading can be determined by $(1 - d_t)E_o$. When the element is compressed, the parameter w_c determines its elastic behaviour, and $(1 - d_t + w_c d_t)E_o$ presents the modulus of elasticity in compression. It is necessary to note that the stiffness in compression is not influenced by cracks (i.e. w_c parameter equals unity). On the other hand, when full degradation and compression stiffness become equal to the stiffness in tension, then the parameter w_c equals zero. Similarly, the damage in compression can be described by the parameter d_c (which defines loses in initial properties that occur in crushing section), while the parameter w_t defines initial properties in tension. Hence, Figure 8 shows both the tension and compression damage parameter curves for estimating stiffness degradation during cyclic loading.

Figure 8: *Concrete damage properties: (a) compression damage, (b) tension damage.*

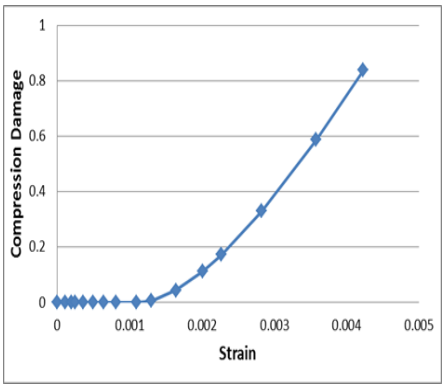

(a)

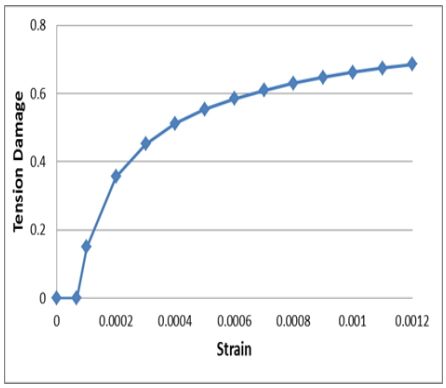

(b)

Steel Reinforcement

The elastic-plastic bilinear kinematic hardening model was utilized for steel reinforcement. This model adequately accounts for the Bauschinger effect. This is defined as a reduced yield stress upon cyclic loading, after plastic strain has been reach during the initial loading. This Bauschinger effect decreases with continued cycling. The true stress and true strain values were then inserted in the plastic option input of the ABAQUS software.

Carbon Fibre Reinforced Polymer

The CFRP composite strip was modelled as an orthotropic elastic material, and the stress-strain relationships can be expressed thus;

$$\begin{bmatrix}\sigma_1\\ \sigma_2\\ \sigma_3\\ \tau_{12}\\ \tau_{13}\\ \tau_{23}\end{bmatrix} = \begin{bmatrix} D_{1111} & D_{1122} & D_{1133} & 0 & 0 & 0 \\ & D_{2222} & D_{1212} & 0 & 0 & 0 \\ & & D_{3333} & 0 & 0 & 0 \\ & & & D_{1212} & 0 & 0 \\ & & Sym. & & D_{1313} & 0 \\ & & & & & D_{2323} \end{bmatrix} \begin{bmatrix}\varepsilon_{11}\\ \varepsilon_{22}\\ \varepsilon_{33}\\ \gamma_{12}\\ \gamma_{13}\\ \gamma_{23}\end{bmatrix} \quad (8)$$

where the stiffness matrix consists of nine independent elastic stiffness parameters (D_{ijkl}), which were defined as shown in Equations (9.1)-(9.8) [10];

$$D_{1111} = E_1(1 - \nu_{23}\nu_{32})\Upsilon, \quad (9.1)$$

$$D_{2222} = E_2(1 - \nu_{13}\nu_{31})\Upsilon, \quad (9.2)$$

$$D_{3333} = E_3(1 - \nu_{12}\nu_{21})\Upsilon, \quad (9.3)$$

$$D_{1122} = E_1(\nu_{21} - \nu_{31}\nu_{23})\Upsilon = E_2(\nu_{12} - \nu_{32}\nu_{13})\Upsilon, \quad (9.4)$$

$$D_{1133} = E_1(\nu_{31} - \nu_{21}\nu_{32})\Upsilon = E_3(\nu_{13} - \nu_{12}\nu_{23})\Upsilon, \quad (9.5)$$

$$D_{2233} = E_2(\nu_{32} - \nu_{12}\nu_{31})\Upsilon = E_3(\nu_{23} - \nu_{21}\nu_{13})\Upsilon, \quad (9.6)$$

$$D_{1212} = G_{12}, \quad D_{1313} = G_{13}, \quad D_{2323} = G_{23} \quad (9.7)$$

$$\Upsilon = \frac{1}{1-\nu_{12}\nu_{21}-\nu_{23}\nu_{32}-\nu_{31}\nu_{13}-2\nu_{21}\nu_{32}\nu_{13}} \quad (9.8)$$

Modelling of Interaction

In the current study, the bond interface behaviour between the CFRP composite strip and the concrete slab was also modelled in ABAQUS, using the cohesive surface interaction approach. This approach was applied for modelling a very thin layer that can be assumed to have zero thickness in practice (e.g. glue). The constitutive response of the cohesive surface interaction approach depends on traction-separation-based response (Figure 9). The damage modelling that defines the traction–separation-based response is described in 4.4.1-4.4.2.

Figure 9: *Typical traction-separation response. [10]*

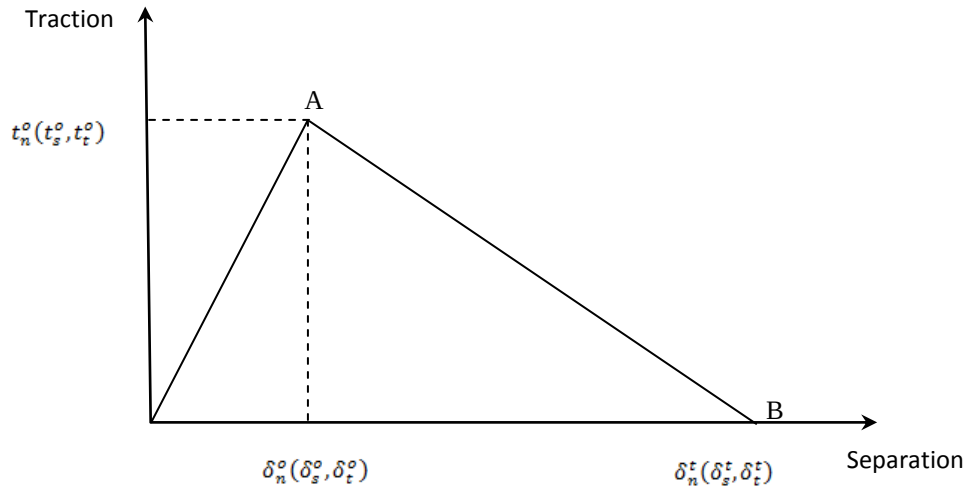

Damage Initiation

Damage initiation was applied based on the maximum nominal stress criterion which is available in ABAQUS. When the maximum nominal stress ratio equals unity, then damage is assumed to initiate, as shown by Equation (10).

$$max\left\{\frac{\langle t_n \rangle}{t_n^0}, \quad \frac{t_s}{t_s^0}, \quad \frac{t_t}{t_t^0}\right\} = 1 \tag{10}$$

Damage Evolution

Once the damage initiation criterion is met, the damage evolution law commences. This however implies that the rate at which cohesive stiffness starts to degrade is based on the scalar damage variable D (which was done by defining the fracture energy required to fully degrade the bond). The contact stress components in the normal, first and second directions between points A and B (Figure 9) are affected by the damage according to the following functions (Equations (11.1)-(11.3);

$$t_n = (1 - D)\overline{t_n} \tag{11.1}$$

$$t_s = (1 - D).\bar{t}_s \tag{11.2}$$

$$t_t = (1 - D).\bar{t}_t \tag{11.3}$$

Where, $\bar{t}_n$, $\bar{t}_s$ and $\bar{t}_t$ are the contact stress components predicted by the elastic traction-separation behaviour for the current separations without damage. It should be noted that Equations (11.1)-(11.3) are only applicable under tension.

Validation of the Finite Element Results

The validation of the present FE predictions in terms of ultimate load, mid-span deflection and ultimate strain in steel and CFRP are compared with the experimental results (Table 3). Table 3 indicates that the ratio of FE predictions to experimental ultimate load ranges from 0.896 to 1.001 with a standard deviation of 0.057. The experimental and FE prediction results in terms of load to mid-span deflection curves obtained for selected slabs are also shown in Figure 10, where it can be observed that the experimental results and FE predictions are in conformance throughout the entire loading range.

Table 3: *Comparison of the predicted and Experimental Results*

Code	Experimental				Numerical				Accuracy
	Ultimate load P_{max} *(KN)*	Mid-span deflection *f (mm)*	Ultimate strain in steel ε_s%	Ultimate strain in CFRP ε_f%	Ultimate load P_{max} *(KN)*	Mid-span deflection *f (mm)*	Ultimate strain in steel ε_s%	Ultimate strain in CFRP ε_f%	P_{num}/P_{exp}
S-T1L0	136	110	> 0.1	NA	136.236	114.73	0.14	NA	1.001
S-T1L1	210	68	0.2	0.8	191.106	63.743	0.472	0.64	0.91
S-T1L2	302	86.2	0.7	*	270.615	89	0.66	0.82	0.896

Figure 10: *Comparison of predicted and experimental load-Mid-span deflection curves.(a) S-T1L0, (b) S-T1L1, (c) S-T1L2.*

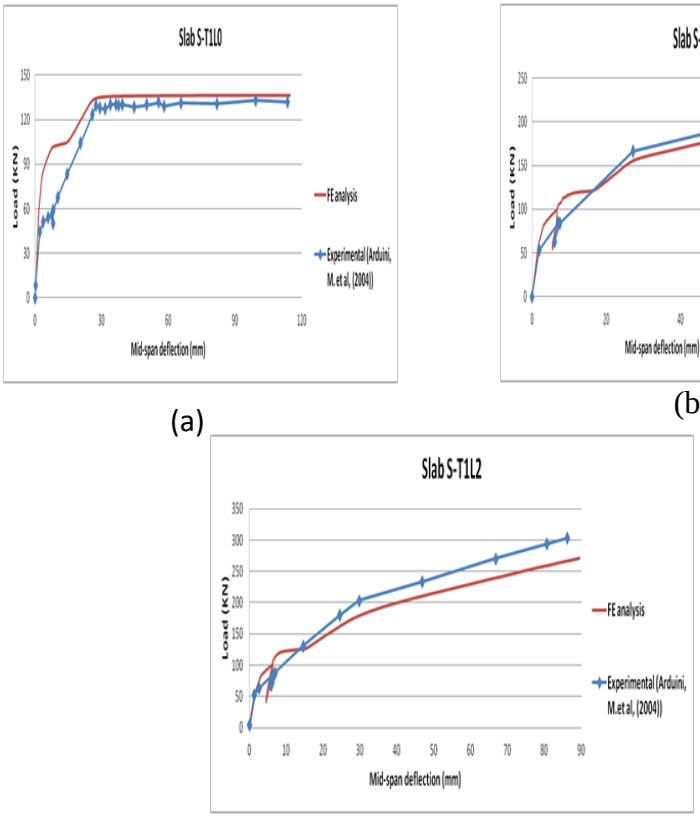

FE Results Based on Modefied FEMA461 Load Protocol

Behaviour of Load versus Mid-Span Deflection

In order to assess the damage accumulation due to the effect of cyclic loading, the numerical results in terms of load versus mid span deflection curves were recorded under monotonic loading and under cyclic fatigue loading using the FEMA 461 modified load protocol (Figure 11). The ultimate load in the monotonic response of slab S-T1L0 is significantly higher than the ultimate load in the fatigue response when compared with the other two slabs (i.e. S-T1L1 & S-T1L2). This is because the effect of repeated load cycles on the slabs' stiffness is less than the effect of added CFRP. Hence, Figure 11 shows that the mid-span deflection of the unstrengthened slab (S-T1L0) exhibits a higher deflection than the slabs strengthened with 800 mm (S-T1L1) and 1500 mm (S-T1L2) width of CFRP respectively (i.e. increase in CFRP contact area with concrete reduces the ductility of the specimen). The specimens have the same failure modes as observed experimentally i.e steel yielding (S-T1L0) and FRP rupture (S-T1L1 & S-T1L2)

Figure 11: *Comparison monotonic and cyclic load-Mid-span deflection. (a) S-T1L0 (b)S-T1L1, (c) S-T1L2.*

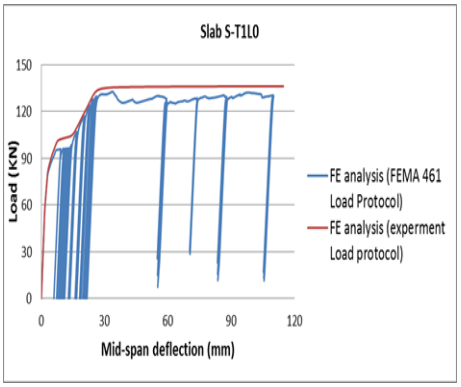

(a)

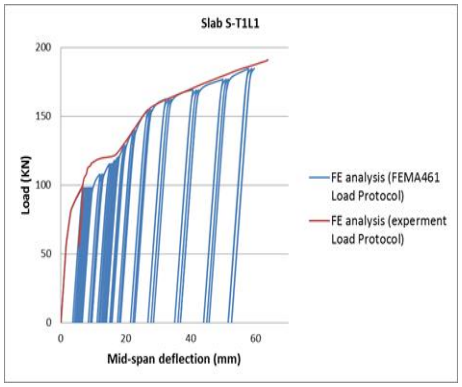

(b)

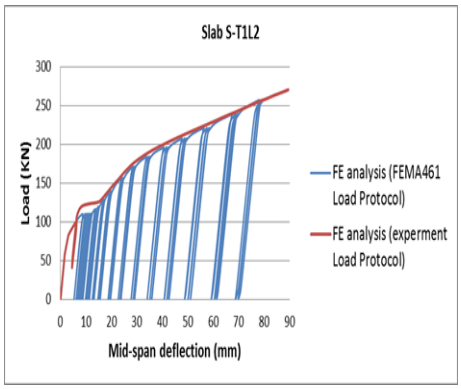

(c)

Figures12-13 show that the CFRP has a power relationship with the cumulative stiffness degradation and the ultimate load reduction percentage. The cumulative stiffness degradation is defined as the summation of stiffness degradation for each stage, where the stiffness degradation is calculated as a difference between the initial and final stiffness. Also, the stiffness was estimated by measuring the slope (i.e. the upper load versus mid-span deflection in a specific cycle). The cumulative stiffness degradation was found to be gradually increasing with increasing cumulative fatigue damage, which is defined as [13];

$$\text{Cumulative Fatigue Damage (CFD)} = \frac{\sum_{j=1}^{i} N_j \cdot \Delta_j^2}{\sum_{j=1}^{n} N_j \cdot \Delta_j^2} \text{X } 100 \qquad (12)$$

where N_j is the number of cycles in different test stages; N_1 = 10, $N_2 = N_3$, ..., N_n = 3.

In the early stages of the modified load protocol, a significant loss of stiffness was observed. As the intensity of cyclic loading increased, the stiffness degradation correspondingly decreased and eventually levelled off. The cumulative stiffness degradation at the end of FEMA 461 load protocol spanned from 0.81 (S-T1L0 slab) to 0.62 (S-T1L2 slab), while the ultimate load reduction percentage spanned from 4.70% (S-T1L0) to 0.1% (S-T1L2).

Figure 12: *Cumulative fatigue damage versus cumulative stiffness degradation*

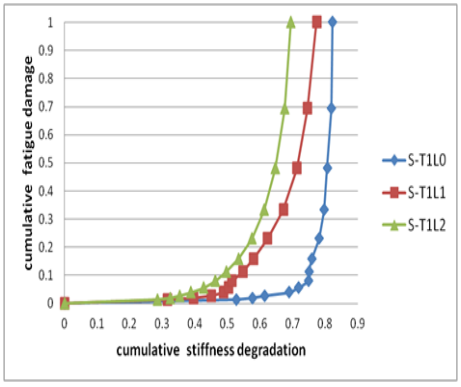

Figure 13: *Percentage of ultimate reduction versus CFRP ratio*

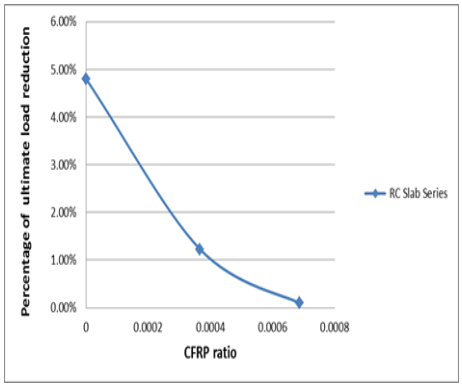

Interfacial Slip Profile

Figures. 14(a)-(b) show a comparison of the interfacial slip profile results in monotonic loading against the results obtained from the modified FEMA 461 load protocol at four different load levels for S-T1L1 and S-T1L2 respectively. The interface slip is estimated as the difference in horizontal displacement (i.e. in the longitudinal direction) between the adjacent FE nodes in the tension side of the concrete slab and the CFRP layer.

Figure 14: *Comparison of slip profile at monotonic and cyclic loading. (a)S-T1L1, (b) S-T1L2*

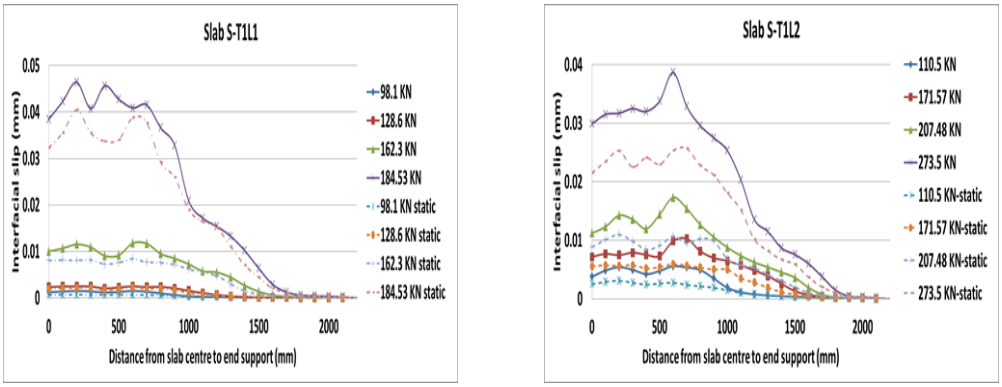

(a) (b)

This comparison illustrates that the predicted interfacial slip values for the slabs tested under the modified FEMA461 load protocol are higher than those of the specimens tested under the monotonic load protocol. It has also been shown that the difference between the interfacial slip profiles of two different load protocols are increased significantly with increased load levels. This is due to the fact that there is a gradual loss of stiffness for concrete, steel and interface bond resulting from cyclic loading. In these interfacial slip profiles, slip was observed to vary from the centre of the slab to the end support (Figure 14). This corresponds to the areas of maximum tensile plastic strain in the concrete (i.e. point of line load application) and region of increasing interfacial slip. This observation suggests that separation should be initiated in the region between two line loads and then propagates towards the ends of the support, which is in agreement with a contour plot (Figure 15) for the damage initiation criterion at the CFRP/concrete interface at failure.

Figure 15: *Contour plot of the damage initiation criterion at the CFRP/concrete interface for slabs (a) S-T1L2 under monotonic loading & (b) S-T1L2 under cyclic loading at failure.*

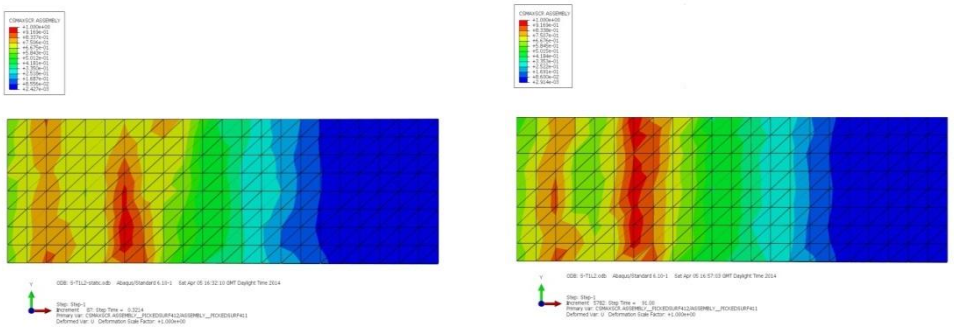

(a) (b)

According to The legend; the red colour shows that the maximum nominal stress criterion has been satisfied and transfer of stress among CFRP and concrete has started to gradually reduce until debonding occurs, whereas the blue colour shows that the CFRP sheet is still bonded to the tension side of concrete slab. It is clear that the damaged region for both slabs (S-T1L1 &S-T1L2) is corresponding to the area of the maximum tensile plastic strain in the concrete substrate.

Tensile Strain Profiles Along FRP

Predicted tensile strain distribution along CFRP in monotonic loading as well as in the modified FEMA 461 load protocol at four different load levels for S-T1L1 and S-T1L2 are shown in Figures 16(a)-(b), respectively. The figures clearly indicate that during early load levels, the strain profiles are linear. Upon increasing the load levels, the strain profiles then begin to fluctuate due to flexural cracks that occurred in the tension side of the RC one way slabs. As earlier mentioned (Figures 14), when the load levels increase, the predicted tensile strains in the longitudinal direction of CFRP (corresponding to the specimens subjected to modified FEMA461 load protocol) become much greater than the specimens subjected to monotonic loading. Also, the strain profiles show that the negligible strains near the end support indicate that the CFRP is adequately anchored (i.e. effectively no slip at its end). In both RC one way slabs (S_T1L1 & S-T1L2), the recorded strain corresponding to the ultimate load capacity in the cyclic loading case is 7000 & 9800 microstrain respectively, which represent only 46% and 64% of their respective full strengths.

Figure 16: *Comparison of slip profile at monotonic and cyclic loading. (a)S-T1L1, (b) S-T1L2.*

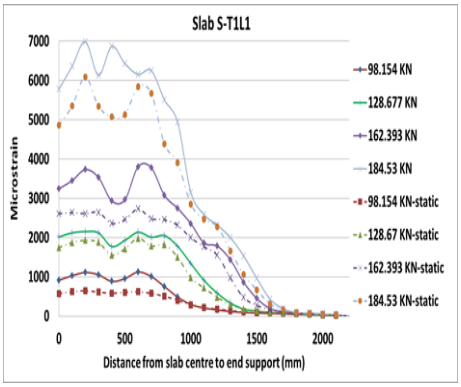

(a)

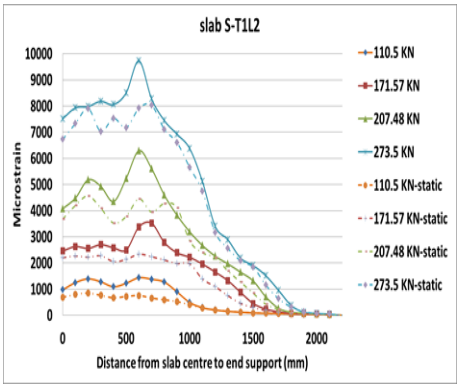

(b)

Conclusions

The current study has developed a three-dimensional finite element model of CFRP-strengthened RC slabs under cyclic loading. The model was also validated with the findings from an earlier experimental study in terms of ultimate load, mid-span deflection and ultimate strain in steel and CFRP. The validation is quite accurate in terms of predicting the overall behaviour. From this basis, the current study introduces the cumulative stiffness degradation of RC during the applied modified FEMA 461 cyclic load protocol, where it was observed that the stiffness degradation is enhanced with increased amount of external reinforcement. Also, the suggested 3-dimensional finite element model introduces a more realistic model for capturing the interface slip profile of composite sheets with the concrete slab during different cyclic stages of loading (which is difficult, if not impossible experimentally).

References

[1] Seim, W., Hörman, M., Karbhari, V., & Seible, F. (2001). External FRP poststrengthening of scaled concrete slabs. *Journal of Composites for Construction*, *5*(2), 67-75.

[2] Ebead, U., & Marzouk, H. (2004). Fiber-reinforced polymer strengthening of two-way slabs. *ACI Structural Journal*, *101*(5).

[3] Hörmann, M., Menrath, H., & Ramm, E. (2002). Numerical investigation of fiber reinforced polymers poststrengthened concrete slabs. *Journal of engineering mechanics*, *128*(5), 552-561.

[4] Kim, Y. J., Longworth, J. M., Wight, R. G., & Green, M. F. (2008). Flexure of two-way slabs strengthened with prestressed or nonprestressed CFRP sheets.*Journal of Composites for Construction*, *12*(4), 366-374.

[5] Robertson, I. N., & Johnson, G. (2004). Repair of slab-column connections using epoxy and carbon fiber reinforced polymer. *Journal of Composites for Construction*, *8*(5), 376-383.

[6] Kotynia, R., Walendziak, R., Stoecklin, I., & Meier, U. (2010). RC slabs strengthened with prestressed and gradually anchored CFRP strips under monotonic and cyclic loading. *Journal of Composites for Construction*, *15*(2), 168-180.

[7] Elsayed, W., Ebead, U. A., & Neale, K. W. (2007). Interfacial behavior and debonding failures in FRP-strengthened concrete slabs. *Journal of Composites for Construction*, *11*(6), 619-628.

[8] Elsayed, W. (2008). Strengthening of Reinforced Concrete Two-Way Slabs Using Mechanically Fastened FRP Systems. Doctoral thesis, Univ. de Sherbrooke, Sherbrooke, Québec, Canada.

[9] Abdullah, A. *(*2010). Analysis of Repaired/Strengthened R.C. Structures Using Composite Materials: Punching Shear. Doctoral Thesis, University of Manchester, UK

[10] ABAQUS (2011). Theory Manual, User Manual and Example Manual, Version 6.10, Providence, RI.
[11] Arduini, M., Nanni, A., & Romagnolo, M. (2004). Performance of one-way reinforced concrete slabs with externally bonded fiber-reinforced polymer strengthening. *ACI Structural Journal*, *101*(2).
[12] Reddy, J. N. (2004). Mechanics of laminated composite plates and shells: theory and analysis. CRC press.
[13] FEMA 461 (2007), Interim Testing Protocols for Determining the Seismic Performance Characteristics of Structural and Non-structural Components. US Department of Homeland Security, Federal Emergency Management Agency, NEHRP
[14] Eurocode 2 (2004). Design of concrete structures: BS EN 1992-1-1and BS EN 1992-1-2. British Standards Institution, London, UK
[15] Wang, T., & Hsu, T. T. (2001). Nonlinear finite element analysis of concrete structures using new constitutive models. *Computers & Structures*, *79*(32), 2781-2791.
[16] Tyau, J. S. *(*2009). Finite Element Modelling of Reinforced Concrete Using 3- Dimensional Solid Elements with Discrete Rebar. Master Thesis, Brigham Young University, USA.